Infrared Spectra and Quantum-Chemical Studies of Disilylmethanes

Donald C. McKean*

School of Chemistry, University of Edinburgh, West Mains Road, Edinburgh EH9 3JJ, U.K.

Received: February 10, 2003; In Final Form: June 2, 2003

New infrared data are reported for disilylmethane-d_0 and -d_6 in the gas phase. Quantum-chemical (QC) calculations have been carried out at HF, MP2, and B3LYP levels with a variety of basis sets. These verify the previously obtained experimental C_{2v} structure. The two possible kinds of SiH bonds are identical in strength but not in electrical properties. Reassignments are made of several vibration frequencies. The A_2 and B_2 torsional frequencies are estimated to be 78.5 and 133 cm^{-1}, respectively, from combination and difference bands. QC-based force fields scaled with 14 factors are used to predict unknown or uncertain frequencies. Scale factors for the A_2 torsion are highly variable with level and basis. By contrast, similar QC calculations of torsional frequencies in disilane, methyl-, fluoro-, chloro-, and ethyl-silanes show very little variation. Stretch/stretch interaction constants between SiH bonds in different silyl groups correlate well with the dipole−dipole energies derived from the QC calculations. Electrical properties of the SiH bond are compared across a range of SiH-containing compounds. A survey of CH stretch/CH stretch interaction force constants in 17 molecules containing CH_3 or CH_2 groups indicates that MP2 calculations are unlikely to be suitable for close analyses of the stretching frequencies of these groups.

Introduction

The complete vibrational spectrum of disilylmethane [$(SiH_3)_2CH_2$], hereafter DSM, was last studied in 1970,[1] since when only the SiH stretching region has been reexamined.[2] The lack of resolution in the earlier work means that a number of aspects of the spectra remain to be clarified, for which purpose a reliable general force field is essential. This can be provided by a good quality ab initio or DFT treatment. The structural interest in DSM in the past has tended to focus on the SiCSi angle which by electron diffraction (ED)[3] or microwave spectroscopy (MW)[4] is somewhat wider than tetrahedral (ED, 114.4(2)°; MW, 114.1(6)°) in a C_{2v} structure, Figure 1, which in other respects resembles that of propane. There is no indication in the MW investigation of a twisting of the silyl groups away from a staggered configuration which characterizes the structures of tri- and tetrasilylmethanes,[5,6] for which a companion QC study has been made.[7] Technical interest in the silylmethanes generally has been stirred by their possible use in the preparation of thin films by chemical vapor deposition.[5,6]

Another structural aspect is the extent to which the two kinds of SiH bonds present can be said to be equivalent. The simplest source of such information is the spectrum of the partially deuterated species $(SiHD_2)(SiD_3)CH_2$, where the solitary SiH bond lies in either the skeletal plane (H^s) or above/below this plane (H^a), leading to the possibility of two isolated SiH stretching frequencies $\nu^{is}SiH^s$ and $\nu^{is}SiH^a$. Observation of only a single $\nu^{is}SiH$ band suggested that the two kinds of bonds were identical in strength.[2] In attempts to interpret both the $\nu^{is}SiH$ value and the SiH stretching frequencies of the parent molecule, long-range dipole−dipole forces acting between the stretching motions of SiH bonds in the two silyl groups were invoked.[2] The presence of such forces acting between SiH bonds similarly disposed has been predicted by quantum-chemical (QC) calculations in several HSiNSiH systems,[8−10] where it has been associated with the substantial negative charge associated with the moving hydrogen atom in an SiH bond. This moving charge is the source of the high SiH stretching infrared intensities typical of SiH compounds, whose variations determined experimentally in methylsilanes correlate very well with those computed in QC calculations.[11]

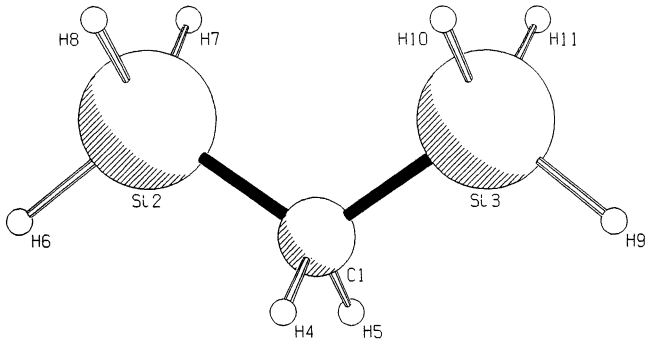

Figure 1. C_{2v} structure of disilylmethane, showing atom numbering.

The latter also show a close link between the static charge on the hydrogen atom as measured by the Mulliken charge and the charges associated with stretching and bending motions of the SiH bonds.[11] The possibility of such a connection in DSM has the added interest that in principle two chemically distinct kinds of SiH bond are present.

Experimental Section

Samples of $(SiH_3)_2CH_2$ (DSM-d_0) and $(SiD_3)_2CH_2$ (DSM-d_6) were available from earlier work[2] and were refractionated before use. Infrared intensities indicated that the concentration of H in d_6 was about 2 atom %.

Mid-infrared spectra were recorded on a Nicolet 7199 FTIR instrument at a resolution of 0.25 cm^{-1}. Approximate intensity data were obtained which will be reported elsewhere.[12]

* To whom correspondence should be addressed. E-mail: dcmck@holyrood.ed.ac.uk.

10.1021/jp030178i CCC: $25.00
Published on Web 08/05/2003

Theoretical Section

Calculations were performed with the program Gaussian 98[13] under the conditions of previous studies[11] ("tight" condition for convergence, density functional calculations using 99 shells, 302 angular points per shell). At the HF, MP2, and B3LYP levels, the bases 6-31G* (hereafter "*sυ*") and 6-311G** (hereafter "*tz*") were employed. The basis 6-311++G** (hereafter "*tz*+"), which includes diffuse functions, was used at the MP2 and B3LYP levels, whereas a single B3LYP/cc-pVTZ[14] (hereafter "B3LYP/*cc*") calculation was also carried out.

The Gaussian 98 output of geometry and Cartesian force constants was input into the program ASYM40[15] for the calculation of symmetry internal force constants and their subsequent scaling to observed frequencies according to the procedure recommended by Pulay et al.[16]

In this type of program, the off-diagonal symmetry force constants are scaled by the geometric mean of the corresponding diagonal constants, an assumption which is hard to justify on theoretical grounds. Instances of a breakdown in this assumption are not uncommon.[17−19] However, the existence of such a breakdown can only be detected by showing that scaling with a maximum number of diagonal scale factors fails to give a satisfactory fit to the range of frequency data available.

Although a "broad brush" approach to scaling, using a limited number of scale factors, is often employed,[20] such an approach is not suited to the detailed reproduction of the experimental frequencies of a particular molecule. The latter can be a valuable source of information regarding small Fermi resonances.

The failure of a simple approach to scaling may be seen in different ways. The use of a single factor for the stretching constant of a particular type of CH or SiH bond rarely succeeds in reproducing accurately the small but precise differences in ν^{is}CH or ν^{is}SiH values found for these bonds, either in the same molecule or in related ones.[18−22] Differing scale factors are then needed. More dramatic instances are the markedly different scale factors needed for the symmetric and antisymmetric SiN stretching force constants in $N(SiH_3)_3$[19] and $MeN(SiH_3)_2$.[23]

Similar considerations apply to the bending modes of CH_3, CH_2, and SiH_3 groups.[18,24,25]

It has been argued that the merit of a particular scaled QC force field is as much to be judged by the range of scale factors it requires as by the extent of their departure from unity.[11,18,23,25,26] This can only be properly assessed if a large number of factors is determined independently for each molecule. The transfer of factors from one molecule to the next should be regarded with suspicion.

Experimental Results

A complete listing of the new infrared frequencies obtained in this work is given in the Supplementary Tables S1 and S2 for the d_0 and d_6 isotopomers, respectively. Two weak bands at 3103 and 1262 cm^{-1} in the d_0 spectrum, both seen before,[1] had unusual contours and may be due to impurity. The d_6 spectrum contained the usual d_5 impurity bands. Table 1 shows frequencies obtained in the νSiH and νSiD regions from these species, including those assigned as combination and differences involving νSiH and SiH_3 torsional levels, shown in Figure 2. Other fundamental frequencies used in the scaling of the force fields are included in Table 2. The silyl deformation regions are shown in Figures 3 and 4 for d_0 and d_6, respectively.

Problems of assignment arise throughout the spectra, discussion of which depends critically upon assistance from the QC calculations, whose results must first be presented.

Figure 2. Infrared spectrum of DSM-d_0 in the νSiH region, showing combination and difference bands involving torsional frequencies. Partial pressure of sample, 70 Torr in a 12 cm cell.

TABLE 1: Infrared Frequencies Observed in the νSiH and νSiD Regions of DSM-d_0 and -d_6 in the Gas Phase

ν_{obs}[a]	assignment
	d_0
2303? sh	$\nu_2 + \nu_{27} + \nu_{14} - \nu_{14}$
2298 sh, C	$\nu_2 + \nu_{27}$
2291? sh, C	$\nu_2 + 2\nu_{27} - \nu_{27}$
2244.5 sh, C	$\nu_{16} + \nu_{14} + \nu_{27} - \nu_{27}$
2242.8 sh, C	$\nu_{16} + \nu_{14}$
2240.8 sh, C	$\nu_{16} + 2\nu_{14} - \nu_{14}$
2268.1 s, C	ν_{23} (b_2)
2167.0 s, q	hot band
2164.1 s, A	ν_{15} (b_1)
2162.5 s, q	ν_{16} (b_1) or hot band
2087 sh, C	$\nu_{16} + \nu_{14} - 2\nu_{14}$
2084 sh, C	$\nu_{16} - \nu_{14}$
2082 sh, C	$\nu_{16} + \nu_{27} - \nu_{14} - \nu_{27}$
2040 sh, C	$\nu_2 + \nu_{27} - 2\nu_{27}$
2033.7 sh, C	$\nu_2 - \nu_{27}$
2029 sh, C	$\nu_2 + \nu_{14} - \nu_{27} - \nu_{14}$
	d_6
2164.6 s, A/C	ν^{is}SiH in $(SiHD_2)(SiD_3)CH_2$
1583.2 s, C	ν_{23} (b_2)
1580.2 s, A	ν_{15} (b_1)
1556.8 ms, A	ν_{16} (b_1)

[a] Intensity indications refer to partial pressures in a 12 cm cell of ~1.7 and ~3.7 Torr respectively for d_0 and d_6.

Theoretical Results

Optimization of the structure at each level with the *sυ* and *tz* basis sets, with constraint only to a C_2 point group, gave the C_{2v} conformation of the microwave investigation, as in Figure 1.[4] Thereafter, a C_{2v} constraint was applied in all calculations. Table 3 compares the geometrical parameters obtained in all of the QC treatments with the MW and ED experimental values. The significantly larger than tetrahedral SiCSi angle observed (MW, 114.1°) is reproduced fairly well at all levels, with a

TABLE 2: QC and Observed Vibrational Data for DSM-d_0 and -d_6

	HF/*tz*			B3LYP/*tz*			HF/*tz*	MP2/*tz*	B3LYP/*tz*	
modes	ν_{uns}[a]	A[b]	R[c]	ν_{uns}[a]	A[b]	ν_{obs}[d]	ϵ_ν[e]	ϵ_ν[e]	ϵ_ν[e]	$-\Delta\nu^{13}$C
						A. $(SiH_3)_2CH_2$				
A_1 ν_1	3151	7	102	3026	3	2907[f]	0.1	15.9	3.3	5.9
ν_2	2338	45	458	2230	125		(2184.6)	(2168.5)	(2167.7)	0.0
ν_3	2319	240	126	2223	80		(2168.3)	(2166.5)	(2166.2)	0.0
ν_4	1522	9	10	1415	8	1369	0.3	0.3	0.3	4.1
ν_5	1061	139	9	969	53		(965.6)	(959.5)	(959.8)	0.0
ν_6	1047	128	41	964	123		(952.4)	(956.9)	(955.5)	0.0
ν_7	827	89	16	768	66		(780.2)	(785.9)	(778.6)	9.3
ν_8	569	1	26	541	1	552	2.0	−1.2	3.1	5.1
ν_9	185	1	0	173	1	173[g]	−2.4	−2.5	−2.4	1.3
A_2 ν_{10}	2314	0	13	2224	0		(2160.7)	(2162.1)	(2161.9)	0.0
ν_{11}	1127	0	4	1059	0	1048.3[h]	0.0	0.0	0.0	0.0
ν_{12}	1042	0	48	963	0		(948.0)	(953.2)	(953.1)	0.0
ν_{13}	617	0	8	576	0		(555.0)	(554.4)	(555.1)	0.0
ν_{14}	76	0	0	81	0	78.5	0.0	0.0	0.0	0.0
B_1 ν_{15}	2328	178	17	2223	13	2164.1[i]	(2175.9)	0.0	0.0	0.0
ν_{16}	2315	94	83	2219	208	2164.1[i]	0.0	(2160.8)	(2159.2)	0.0
ν_{17}	1202	101	2	1111	62	1057.7	0.0	−2.4	−0.1	14.3
ν_{18}	1039	92	0	959	63	947.9	3.1	−2.1	−2.2	0.1
ν_{19}	1015	538	14	926	407	919	−3.4	2.3	2.2	0.3
ν_{20}	802	60	6	764	60	763.4	−2.0	1.8	−3.0	13.1
ν_{21}	622	2	4	574	0	579	−0.6	1.2	−0.8	0.3
B_2 ν_{22}	3194	7	80	3070	3	2946.2	0.0	0.0	0.0	10.4
ν_{23}	2322	341	134	2230	246	2168.1	0.0	0.0	0.0	0.0
ν_{24}	1048	148	3	968	84	952.8	−0.1	−5.5	−5.3	0.0
ν_{25}	899	155	3	835	126	812	0.3	−0.2	1.3	8.6
ν_{26}	489	9	1	463	6	463	0.9	1.3	−0.7	0.6
ν_{27}	143	0	0	136	0	133	0.0	0.0	0.0	0.8
						ΣWSE[j]	1.90	2.26	2.40	
						B. $(SiD_3)_2CH_2$				
A_1 ν_1	3151	6	101	3026	3	2907[f]	0.2	15.9	3.3	5.9
ν_2	1676	158	61	1608	114		(1582.6)[k]	(1581.6)[k]	(1581.2)[k]	0.0
ν_2	1664	15	225	1586	9		(1570.8)[k]	(1559.2)[k]	(1559.0)[k]	0.0
ν_4	1521	10	12	1414	9	1368[l]	−0.3	−0.3	−0.3	4.1
ν_5	801	140	7	738	100	738[f]	−4.2	−2.3	0.4	4.7
ν_6	759	57	14	696	36		(691.5)	(692.3)	(689.3)	0.5
ν_7	704	2	16	658	0	663[f,g]	3.2	−1.4	0.9	8.8
ν_8	490	8	20	462	7	469	0.7	−2.5	1.2	1.1
ν_9	165	1	0	154	1	159[g]	2.8	2.9	2.9	1.0
A_2 ν_{10}	1671	0	6	1606	0		(1576.1)[k]	(1577.5)[k]	(1577.3)[k]	0.0
ν_{11}	1104	0	4	1040	0		(1029.9)	(1029.0)	(1031.2)	0.0
ν_{12}	749	0	21	690	0		(680.7)	(684.1)	(683.7)	0.0
ν_{13}	465	0	6	433	0	417[g]	0.0	0.0	0.0	0.0
ν_{14}	54	0	0	58	0		(55.8)	(55.9)	(55.8)	0.0
B_1 ν_{15}	1672	73	46	1605	46	1580.2[f]	0.5[k]	1.1[k]	1.2[k]	0.0
ν_{16}	1656	94	5	1579	88	1556.8[f]	−5.6[k]	4.2[k]	5.1[k]	0.0
ν_{17}	1189	81	2	1099	50	1045.2	2.0	0.3	1.8	14.9
ν_{18}	808	184	2	766	122	765.5	−1.9	2.7	−2.3	11.8
ν_{19}	747	71	0	689	49	687.8[f]	8.6	5.3	5.2	0.0
ν_{20}	734	157	10	673	151	670.4	0.5	3.8	3.7	1.6
ν_{21}	465	2	2	430	0	434	−0.7	0.4	−0.8	0.0
B_2 ν_{22}	3194	6	81	3070	3	2944.0[f]	−2.2	−2.2	−2.1	10.4
ν_{23}	1678	206	67	1612	148	1583.2[f]	1.0[k]	0.7[k]	0.8[k]	0.0
ν_{24}	811	119	2	758	77	738[f]	1.9	5.2	1.6	9.8
ν_{25}	751	56	2	694	47	687.8[f]	5.5	1.3	1.0	0.2
ν_{26}	414	10	1	389	7	390[g]	−0.1	−1.0	0.0	0.0
ν_{27}	112	0	0	107	0		(104.3)	(103.9)	(104.0)	0.8
						ΣWSE[j]	2.18	2.91	2.55	

[a] Unscaled QC frequency (cm^{-1}). [b] QC infrared intensity (km mol^{-1}). [c] QC Raman scattering activity ($Å^4$ amu^{-1}). [d] Frequency observed in this work, except where otherwise indicated. [e] Frequency fit: $\epsilon_\nu = \nu_{obs} - \nu_{calc}$, or in parentheses, the calculated frequency. [f] Frequency omitted from the refinement. [g] Raman liquid value from ref 1. [h] Solid solution value from ref 1. [i] Refinement is only possible if 2164.1 cm^{-1} is the higher frequency in the MP2 and B3LYP refinements, but the lower one in the HF calculations. [j] ΣWSE = sum of weighted squares of errors, calculated as described in ref 15. [k] Calculated frequency multiplied by 1.01, to offset effect of anharmonicity.[27] [l] Fermi resonance correction applied.

tendency to overestimate with the *tz* basis and at the HF and B3LYP levels. Of particular relevance to the interpretation of the νSiH region of the spectrum are the very small differences in length between the SiH^s and SiH^a bonds. These lengths are quoted to five decimal places to avoid rounding error. (Reproducibility in the optimization procedure is about 0.000 02 Å). Unlike the case of the similarly disposed CH bonds in Me_2SiH_2, where there is good agreement in all calculations on a small positive $CH^a - CH^s$ difference, the variation in sign of the minute differences seen between the SiH^s and SiH^a lengths means that these bonds must be considered to be indistinguishable. The tilt of the silyl group, as measured by the difference between

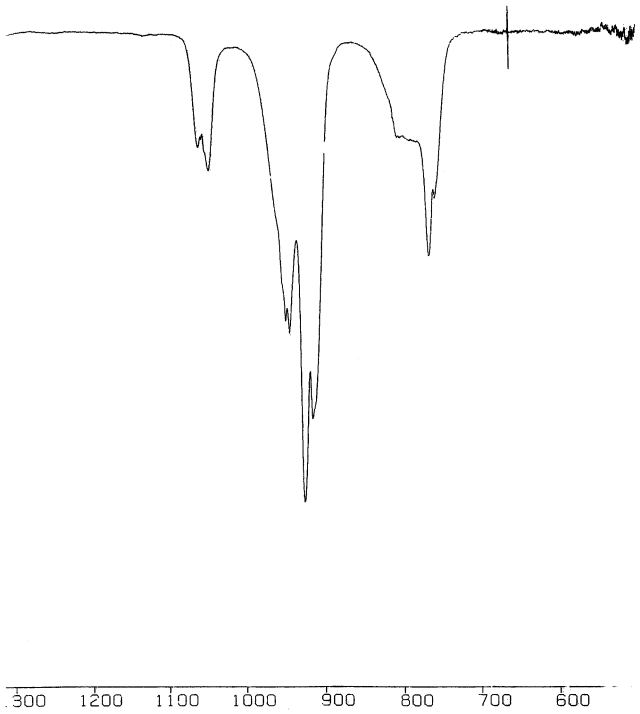

Figure 3. Infrared spectrum of DSM-d_0 in the region 1200−600 cm^{-1}. Partial pressure of sample, 1.8 Torr in a 12 cm cell.

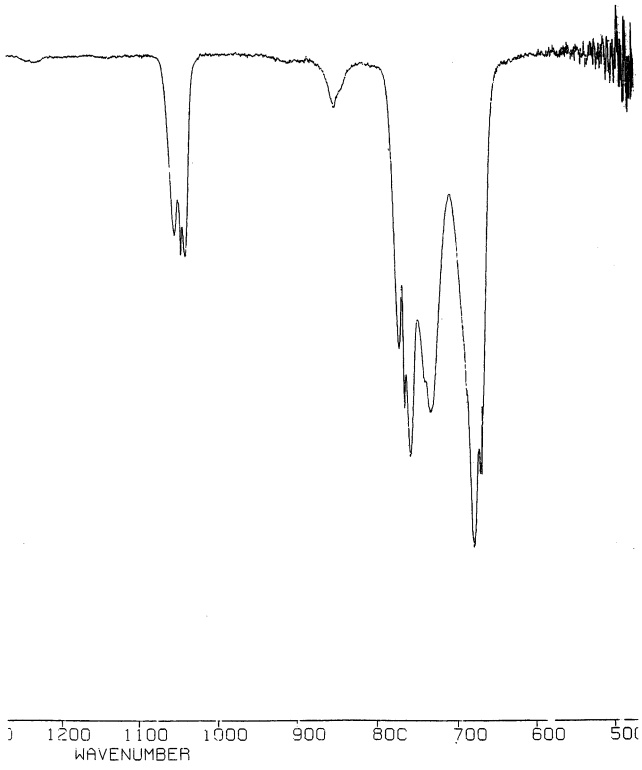

Figure 4. Infrared spectrum of DSM-d_6 in the region 1200−600 cm^{-1}. Partial pressure of sample, 3.8 Torr in a 12 cm cell.

the H^{a}SiC and H^{s}SiC angles, is small or negligible at all levels. A further illustration of this equivalence is provided by the unscaled ν^{is}SiH values calculated in the species $(SiHD_2)(SiD_3)$-CH_2, shown in Table 4. There is a modest sensitivity to basis set, but in all cases the SiH^s bond is only marginally weaker than the SiH^a one.

By contrast the associated intensities are markedly different. The MP2 and B3LYP calculations agree well in predicting a fall of 22−25% in the IR intensity A from SiH^s to SiH^a. There is a similar fall in the Raman scattering activity from the two available calculations, at the HF level.

Table 2 includes the unscaled vibrational data produced by the HF and B3LYP calculations with the *tz* basis, the observed frequencies, and the frequency fit obtained after scaling the HF/*tz*, MP2/*tz*, and B3LYP/*tz* force fields. Only those frequencies considered to be reliable were used in the scaling of the force fields, as detailed below.

Also given in Table 2 are the frequency shifts resulting from ^{13}C substitution in d_0 calculated from the scaled B3LYP/tz force field.

Assignments. Attention is focused on aspects of the spectra unclear in the previous work.

(1) νCH Region. The type C bands at 2946.2 (d_0) and 2944 cm^{-1} (d_6) identify $\nu_{22}(b_2)$ in the two isotopomers, whereas the type B band at 2907 cm^{-1} due to $\nu_1(a_1)$ is well defined in d_0, less well so in d_6. The upper level of the latter is likely to be in weak Fermi resonance with $2 \times \nu_4$ at 2822 cm^{-1}, but the extent of the resonance shift appears to be small, perhaps 6−7 cm^{-1}, judging by the results in Table 2 of scaling both CH stretching symmetry force constants to the value of ν_{22}.

(2) νSiH Region. The large mass of the silicon atom, as compared to that of carbon, means that the composition of stretching modes of the silyl group is the consequence of a delicate balance between opposing G and F matrix terms, such that in-phase stretches may lie above or below out-of-phase ones, depending on the exact size of the valence interaction force constants. (The terms "symmetric" and "antisymmetric" are usually inappropriate in such circumstances). In addition the coupling is markedly affected by small differences in the diagonal valence constants. It is therefore not surprising to find markedly different descriptions of the unscaled frequencies given in Table 5 from the different calculations. In part these differences stem from the differences in ν^{is}SiH value seen in Table 4.

The IR spectrum of d_0 (Figure 4, ref 2) shows clearly identifiable type A and type C bands at 2164.1 and 2168.1 cm^{-1} which must arise from B_1 and B_2 modes, respectively. One of two subsidiary Q branches at 2162.5 and 2167.0 cm^{-1} may represent the other B_1 band expected here or else both of these may be hot bands. In d_6, a single A/C hybrid band at 2164.6 cm^{-1} has the appearance expected from a solitary SiH^a bond in d_5 impurity, but the absence of any sign of a second Q branch suggests that the ν^{is}SiH^s and ν^{is}SiH^a bands in fact coincide. The B_2 fundamental at 2168.1 cm^{-1} has to be ν_{23}. Because its normal coordinate involves the stretching of the SiH^a bonds only, this frequency provides an unambiguous datum for scaling the four symmetry force constants involving SiH^a stretching. However, the B_1 2164.1 cm^{-1} band may represent either ν_{15} or ν_{16}, each of which should involve stretching of both SiH^a and SiH^s bonds. It proved possible to scale the SiH^s stretching symmetry force constants using this second datum but on a different basis for the HF as compared with the MP2 and B3LYP treatments. The HF data only allowed refinement when the B_1 band was taken to be the lower mode, ν_{16}. By contrast, the MP2 and B3LYP treatments required the B_1 band to be ν_{15}. Table 5 shows the resulting predictions for the unassigned νSiH bands, the associated scaled ν^{is}SiH frequencies, and all six of the scaled νSiD frequencies in d_6. The latter have all been multiplied by the factor 1.01 to offset the differing effects of anharmonicity on SiH and SiD stretching frequencies, for a more meaningful comparison with the observed spectrum.[27,28]

A clear choice between the alternative assignments for the 2164.1 cm^{-1} band can then be made by examining the associated

TABLE 3: Comparison of Observed and Calculated Structural Parameters for DSM

			calculated[b]								
	observed		HF		MP2			B3LYP			
parameter[a]	ED[c]	MW[d]	*sv*	*tz*	*sv*	*tz*	*tz*+	*sv*	*tz*	*tz*+	*cc*
r(C−H)	1.11(2)	1.091(15)	1.0892	1.0894	1.0965	1.0966	1.0969	1.0982	1.0960	1.0961	1.0935
∠HCH	110.0[e]	107.3(18)	106.2	106.3	106.6	106.5	106.4	106.5	106.3	106.3	106.5
r(Si−C)	1.873(2)	1.874(12)	1.8885	1.8846	1.8836	1.8790	1.8794	1.8898	1.8881	1.8881	1.8860
∠SiCSi	114.4(2)	114.1(6)	116.4	117.3	114.6	115.8	115.9	115.4	116.5	116.5	116.1
r(Si−H^s)	1.512(6)[f]	1.475(14)	1.47763	1.47962	1.48721	1.47777	1.47804	1.48948	1.48706	1.48711	1.48595
r(Si−H^a)	1.512[f]	1.477(3)	1.47769	1.47995	1.48681	1.47800	1.47838	1.48857	1.48656	1.48667	1.48540
Δr(Si−H)$^{a-s}$	0.000	0.002(14)	0.00006	0.00033	−0.00040	0.00023	0.00034	−0.00091	−0.00050	−0.00044	−0.00055
∠H^{a}SiH^a	108.1(11)[f]	108.6(3)	108.4	108.4	108.5	108.6	108.6	108.3	108.4	108.4	108.4
∠H^{s}SiH^a	108.1[f]	108.1(13)	108.4	108.5	108.4	108.7	108.7	108.2	108.4	108.4	108.4
∠H^{s}SiC	110.8[f]	111.2(8)	110.7	110.5	111.0	110.8	110.9	111.0	110.7	110.7	110.8
∠H^{s}SiC	110.8[f]	111.2(8)	110.7	110.5	111.0	110.8	110.9	111.0	110.7	110.7	110.8
∠H^{a}SiC	110.8[f]	109.9(10)	110.5	110.5	110.2	110.0	110.0	110.6	110.5	110.4	110.4
μ		0.819(2)	0.7868	0.7624	0.7430	0.7720	0.7605	0.8461	0.7930	0.7717	0.8364

[a] Bond lengths are in angstroms, angles are in degrees, and dipole moments μ are in Debye. Atom H^s lies in the skeletal plane of the molecule, and H^a lies above or below this plane. [b] This work. [c] Reference 3. [d] Reference 4. [e] Assumed. [f] C_{3v} local symmetry assumed.

TABLE 4: Unscaled QC Frequencies (cm^{-1}) and Intensities for ν^{is}SiH^s and ν^{is}SiH^a Bands in DSM

	SiH^s		SiH^a			
level/basis	ν^{is}	$A(R)$[a]	ν^{is}	$A(R)$[a]	$\Delta\nu^{is}$ (H^s−H^a)	$\Delta A(R)$ (H^s−H^a)
HF/*sv*	2367.5	227.8(141.3)	2368.8	186.2(95.8)	−1.3	41.6(45.5)
HF/*tz*	2321.9	176.4(176.3)	2322.5	142.3(120.7)	−0.6	34.1(55.6)
MP2/*sv*	2304.8	172.0	2309.8	132.1	−5.0	39.9
MP2/*tz*	2308.7	142.4	2310.0	110.3	−1.3	32.1
MP2/*tz*+	2306.2	144.2	2307.0	111.0	−0.8	33.2
B3LYP/*sv*	2238.6	169.4	2246.0	129.6	−7.4	39.8
B3LYP/*tz*	2221.2	136.9	2226.2	103.7	−5.0	33.2
B3LYP/*tz*+	2220.3	139.7	2225.1	105.0	−4.8	34.7
B3LYP/*cc*	2213.3	133.3	2218.6	98.1	−5.3	35.2

[a] Where available from Gaussian 98. A is the infrared intensity in km mol^{-1}, and R is the Raman scattering activity in Å^4 amu^{-1}.

TABLE 5: QC-Based SiH and SiD Stretching Frequencies (cm^{-1}) after Scaling to ν_{15} or ν_{16} (b_1) = 2164.1, ν_{23} (b_2) = 2168.1 cm^{-1}

A. DSM-d_0

level/basis	$\nu_2(a_1)$	$\nu_3(a_1)$	$\nu_{10}(a_2)$	ν_{16} or $\nu_{15}(b_1)$[a]	ν^{is}SiH^s	ν^{is}SiH^a	$\Delta\nu^{is}$ (H^s−H^a)
HF/*sv*	2185.4	2171.7	2159.5	2178.1	2179.2	2166.8	12.4
HF/*tz*	2184.6	2168.3	2160.7	2175.9	2172.6	2168.8	3.8
MP2/*sv*	2167.1	2162.5	2161.3	2154.2	2164.0	2162.3	1.7
MP2/*tz*	2168.5	2166.5	2162.1	2160.8	2165.1	2164.7	0.4
MP2/*tz*+	2169.2	2166.5	2162.1	2161.5	2165.3	2165.0	0.3
B3LYP/*sv*	2166.9	2164.3	2160.7	2154.7	2164.5	2162.3	2.2
B3LYP/*tz*	2167.7	2166.2	2161.9	2159.2	2164.9	2164.1	0.8
B3LYP/*tz*+	2168.0	2166.3	2161.8	2159.5	2164.9	2164.2	0.7
B3LYP/*cc*	2166.7	2166.2	2161.7	2158.1	2164.6	2163.7	0.9
obs					?	2164.6	?

B. DSM-d_6 (scaled frequencies × 1.01)

level/basis	$\nu_2(a_1)$	$\nu_3(a_1)$	$\nu_{10}(a_2)$	$\nu_{15}(b_1)$	$\nu_{16}(b_1)$	$\nu_{23}(b_2)$
HF/*sv*	1587.5	1569.4	1575.3	1584.3	1559.8	1582.3
HF/*tz*	1582.6	1570.8	1576.1	1579.7	1562.4	1582.2
MP2/*sv*	1582.1	1555.4	1577.2	1579.3	1548.1	1582.8
MP2/*tz*	1581.6	1559.2	1577.5	1579.1	1552.6	1582.5
MP2/*tz*+	1581.5	1559.7	1577.4	1579.0	1553.1	1582.5
B3LYP/*sv*	1581.8	1557.1	1576.6	1579.0	1548.9	1582.7
B3LYP/*tz*	1581.2	1559.0	1577.3	1579.0	1551.7	1582.4
B3LYP/*tz*+	1581.2	1559.2	1577.2	1579.0	1551.9	1582.4
B3LYP/*cc*	1581.2	1558.2	1577.2	1578.9	1551.0	1582.4
obs	?	?	?	1580.2	1556.8	1583.2

[a] ν_{15} for the HF calculations, ν_{16} for all of the others.

ν^{is}SiH values. The MP2 and B3LYP scaled ν^{is}SiH values lie close to each other and also to the Q branch observed at 2164.6 cm^{-1}, whereas both HF ν^{is}SiH values lie unacceptably high, at 2172.6 (H^s) and 2168.8 (H^a) (*tz* basis) or 2178.1 and 2166.8 cm^{-1} (*sv* basis).

A further argument for assigning the 2164.1 cm^{-1} Q branch to ν_{15} comes from using a bond dipole model to predict the relative intensities of the two modes. Both MP2 and B3LYP approaches indicate that ν_{15} is primarily a motion of the two SiH^s bonds, whereas ν_{16} derives largely from ν_sSiH$^a_2$ stretching

TABLE 6: Comparison of Calculated and Observed Torsional Frequencies in Some Compounds Containing Silyl Groups[a]

	DSM		DS	MS	FMS	CMS	ETS	
level/basis	$\nu_{14}(a_2)$	$\nu_{27}(b_2)$	$\nu_{12}(a_{1u})$	$\nu_6(a_2)$	$\nu_{18}(a'')$	$\nu_{18}(a'')$	$\nu_{27}(a'')$	$\nu_{26}(a'')$
HF/*sv*	69.1	144.0	133.0	193.6	157.6	157.2	137.9	235.2
HF/*tz*	75.7	142.6	134.7	197.9	154.5	158.9	141.2	234.3
MP2/*sv*	47.8	145.7	140.4	201.7	169.4	161.8	142.1	235.8
MP2/*tz*	56.7	139.0	147.6	196.0	158.1	159.9	136.0	232.4
MP2/*tz*+	44.9	141.1	146.6	199.6	148.9	156.1	135.3	225.0
B3LYP/*sv*	73.1	136.1	129.7	192.3	161.3	153.7	137.3	226.0
B3LYP/*tz*	81.0	136.3	135.4	193.9	154.4	155.5	139.9	220.8
B3LYP/*tz*+	77.9	135.2	131.5	192.4	151.0	154.0	139.0	220.0
B3LYP/*cc*	85.8	139.6						
obs	78.5	133	125.5[b]	190[c]	149[d]	161[e]	132[f]	207[f,g]

[a] DSM = disilylmethane; DS = disilane; MS = methylsilane; FMS = FCH_2SiH_3; CMS = $ClCH_2SiH_3$; ETS = ethylsilane, where $\nu_{27} = \tau SiH_3$, $\nu_{26} = \tau CH_3$. This work, except where otherwise indicated. [b] Reference 29. This value is exactly one-half of the frequency of the $2 \leftarrow 0$ transition quoted earlier,[30] which is surprising for a strongly anharmonic situation. [c] Reference 31. [d] Reference 32. [e] Reference 33. [f] Reference 34. [g] Value from solid-state spectra.

motion. The bond dipole model then predicts that ν_{15} will produce a more intense band than ν_{16}. In the latter, the change of moment in each silyl group lies almost exactly along the C_2 symmetry axis, with only a small component along the *A* inertial axis. The resultant dipole change is therefore small. The SiH^s bond, by contrast, is directed within 33° of this axis, so that the resultant dipole change is large. We conclude that ν_{16} lies below 2164.1 cm^{-1}, the best predictions being those from the MP2/*tz* and MP2/*tz*+ calculations, 2160.8 and 2161.5 cm^{-1}, respectively. These are sufficiently close to the Q branch at 2962.5 cm^{-1} for the latter to be a strong candidate for ν_{16}. As such, it provides a reasonable interpretation of the torsional combination and difference bands, as detailed below. At all events, it can safely be concluded that the fourth Q branch at 2167.0 cm^{-1} derives from a hot band.

Assignment of the combination and difference bands involving νSiH and τSiH_3 levels listed in Table 1 must now be considered. These bands are seen as very weak sharp shoulders on each side of the intense νSiH absorption in Figure 2, which indicate the presence of type C bands. Table 6 lists the unscaled predictions for the torsional frequencies ν_{14} and ν_{27}, together with similar predictions for some other molecules containing silyl groups. In DSM, there is quite good agreement among the nine calculations on the magnitude of ν_{27}, which is predicted in the range 135−146 cm^{-1}, but a surprising variation in the value of ν_{14}, which ranges from 45 to 86 cm^{-1}. A similar variability in the prediction of silyl torsional frequencies is found in trisilylmethane.[7] By contrast, calculated values of torsional frequencies in disilane (DS), methylsilane (MS), fluoro- and chloromethylsilanes (FMS, CMS), and ethylsilane (ETS), also listed in Table 6, show in general good agreement both between levels of theory and also between theory and experiment.[29−34]

Focusing on the spectrum of DSM, it is clear that the pairs of Q branches 2242.8, 2240.8, and 2087, 2084 cm^{-1} must be associated with the lower torsional frequency $\nu_{14}(a_2)$. Type C bands will result when a quantum of this vibration is associated with a νSiH one of B_1 symmetry. Of the two B_1 candidates, ν_{15} and ν_{16}, ν_{16} is largely an asymmetric stretch of the SiH^a bonds and, as such, seems more likely to interact with torsional motion than the stretching of SiH^s. Assuming ν_{16} to be responsible for the Q branch at 2162.5 cm^{-1}, the tentative assignment is made (Table 1) of 2242.8 and 2084 cm^{-1}, respectively, to the combination and difference bands involving ν_{16} with ν_{14}. This places ν_{14} at 78.5 cm^{-1}. The other Q branches are then assigned to hot bands in ν_{14} and ν_{27}, rather than to levels involving ν_{15}.

Type C combination and difference bands arising from $\nu_{27}(b_2)$ can arise from either of the A_1 modes ν_2 and ν_3, the best predictions for which are about 2169 and 2166.5 cm^{-1} (Table 5). The closest match in appearance lies between the Q branches at 2298 and 2033.7 cm^{-1}, which together fit quite well as combination and differences between ν_3 at about 2166.5 and ν_{27} at about 133 cm^{-1}. The remaining difference bands at 2040 and 2029 cm^{-1} and the very doubtful combinations at 2303 and 2291 cm^{-1} are tentatively assigned as hot bands, as in the discussion of ν_{14} above.

This analysis depends markedly on the reliability of the QC calculations of values of the sretch−stretch interaction force constants f' connecting SiH bonds in the same and in differing silyl groups. This is hard to assess. A final judgment on the assignments of these Q branches must await a more careful investigation at higher resolution in a spectrum which is free of the interference from atmospheric CO_2 absorption visible in Figure 2. However, the present analysis and prior examples such as that of ethylsilane[34] together suggest that torsional modes should normally be identifiable from their combination and difference bands involving SiH stretching quanta. The problem is to discover which νSiH fundamentals are involved in each transition.

(3) νSiD Region. The change here in the relative masses of the silicon and terminal atoms means that in contrast to the SiH region there is a well-defined distinction between higher-lying $\nu_{as}SiD_3$ and lower-lying ν_sSiD_3 modes. The Q branch of the B_2 $\nu_{as}SiD_3$ band ν_{23} is plain at 1583.2 cm^{-1}, whereas type A bands centered at 1580.2 and 1556.8 cm^{-1} identify the B_1 bands due to ν_{15} and ν_{16}. As seen in Table 2, the two bands assigned to ν_{15} and ν_{23} are fitted to within 1 cm^{-1} using the force constants scaled on the d_0 values of ν_{15} and ν_{23} above, plus the usual anharmonicity correction factor of 1.01.[27] However, ν_{16} is predicted not higher than 1553 cm^{-1} (ignoring the HF results, rejected above), which is ~4 cm^{-1} lower than observed. This may reflect the need for a variation in the above anharmonicity correction.

(4) A_2 Modes. In the previous study,[1] the A_2 τCH_2 mode ν_{11} was identified as the weak Raman line at 1101 cm^{-1} in the liquid phase, above the wCH_2 band (ν_{17}) at 1058 cm^{-1}. However, all of the QC unscaled calculations place ν_{11} substantially below ν_{17}, making the above assignment untenable. A plausible position for ν_{11} is the hitherto unassigned sharp feature at 1048.3 cm^{-1} in the solid solution spectrum,[1] its infrared activity being ascribed to a lowering of the symmetry in the crystal phase. The assignment of the weak sharp band in the solid spectrum just below at 1038.4 cm^{-1} as a ^{13}C counterpart of ν_{17} is confirmed by the calculated ^{13}C frequency shifts in Table 2.

Assigning ν_{11} near 1048 cm^{-1} would be likely to render the band indistinguishable from ν_{17} in the liquid-phase Raman spectrum.

TABLE 7: Scale Factors for QC-Based Force Fields for DSM

type	symmetry coordinates[a]	HF/*sv*	HF/*tz*	MP2/*sv*	MP2/*tz*	MP2/*tz*+	B3LYP/*sv*	B3LYP/*tz*	B3LYP/*tz*+	B3LYP/*cc*
νCH	4, 23	0.8319	0.8511	0.8645	0.8792	0.8818	0.9067	0.9209	0.9217	0.9201
$\delta_s CH_2$	9	0.7754	0.8091	0.8629	0.9333	0.9445	0.9008	0.9367	0.9406	0.9424
τCH_2	14	0.8501	0.8723	0.9207	0.9869	0.9953	0.9749	0.9861	0.9894	1.0100
ρCH_2	27	0.8223[b]	0.8400[b]	0.8969[b]	0.9424[b]	0.9447[b]	0.9582[b]	0.9629[b]	0.9666[b]	0.9722[b]
wCH_2	21	0.7033	0.7326	0.8031	0.8646	0.8638	0.8602	0.8791	0.8813	0.9130
νCSi_2	3, 17	0.9473	0.9527	0.9546	0.9530	0.9559	1.0304	1.0285	1.0293	1.0240
δCSi_2	8	0.9153	0.9022	0.9747	1.0277	1.0623	1.0651	1.0222	1.0311	1.0511
νSiH^s	1, 15	0.8473	0.8755	0.8815	0.8796	0.8816	0.9349	0.9500	0.9508	0.9566
νSiH^a	2, 10, 16, 22	0.8367	0.8720	0.8764	0.8783	0.8807	0.9270	0.9450	0.9461	0.9511
$\delta_{as} SiH_3$	5, 11, 18, 24	0.8274[c]	0.8273[c]	0.9238[c]	0.9056[c]	0.9088[c]	0.9882[c]	0.9811[c]	0.9817[c]	0.9874[c]
$\delta_s SiH_3$	6, 19	0.8274[c]	0.8273[c]	0.9238[c]	0.9056[c]	0.9088[c]	0.9882[c]	0.9811[c]	0.9817[c]	0.9874[c]
$\rho' SiH_3$	7, 20	0.8781	0.8753	0.9809	0.9875	0.9884	1.0425	1.0278	1.0269	1.0285
$\rho'' SiH_3\ A_2$	12	0.7971	0.8006	0.8889	0.8934	0.8894	0.9363	0.9232	0.9239	0.9256
$\rho'' SiH_3\ B_2$	25	0.8223[b]	0.8400[b]	0.8969[b]	0.9424[b]	0.9447[b]	0.9582[b]	0.9629[b]	0.9666[b]	0.9722[b]
$\tau SiH_3\ A_2$	13	1.2974	1.0791	2.7577	1.9360	3.1123	1.1581	0.9385	1.0165	0.8355
$\tau SiH_3\ B_2$	26	0.8550	0.8708	0.8294	0.9131	0.8841	0.9531	0.9502	0.9673	0.9029
average[d]		0.8360	0.8509	0.9024	0.9276	0.9331	0.9604	0.9636	0.9658	0.9735
range[d]		0.2440	0.2201	0.1716	0.1631	0.1985	0.2049	0.1494	0.1498	0.1381
σ_n[d,e]		0.0604	0.0533	0.0492	0.0506	0.0576	0.0594	0.0451	0.0456	0.0444
ΣWSE[f]		3.93	4.12	4.86	5.20	4.97	4.45	4.98	5.05	4.57

[a] As defined in Reference 11, with the interchange of silicon and carbon atoms. [b,c] Constrained equal. [d] Excluding τSiH_3. [e] Sample standard deviation. [f] Sum of weighted squares of errors for d_0 and d_6 frequencies.

Apart from a dubious feature at 1113 cm^{-1} in the Raman spectrum of d_6, whose previous asignment to ν_{11} is untenable, the only other Raman feature previously assigned to an A_2 mode is the weak band in d_6 at 417 cm^{-1}. This fits well with the prediction of ~426 cm^{-1} for the ρSiD_3 mode ν_{13} which results from the assumption of equal scale factors for the ρSiD_3 constants in the A_2 and B_2 species. An independent datum for the scaling of the A_2 ρSiD_3 constant is therefore available.

(5) Silyl Deformations. In d_0, these are predicted to lie close to each other near 950 cm^{-1}, except for the very intense B_1 band due to the $\delta_s SiH_3$ mode ν_{19}, expected some 30 cm^{-1} lower. The latter may be confidently assigned to the very strong band with a minimum at 921.5 cm^{-1} and likely center near the maximum at 918.4 cm^{-1}, although no discrete Q branch was discernible. Q branches at 952.8 and 947.9 cm^{-1} are likely to arise from $\nu_{24}(b_2)$ and $\nu_{18}(b_1)$, but the contours here are confusing, as Figure 3 shows. In the d_6 spectrum, Figure 4, apart from the well-defined type A band at 765.5 cm^{-1} due to $\nu_{18}(b_1, \nu_{as}CSi_2)$, the contours are also confusing. The A_1 $\delta_s SiD_3$ mode is displaced above all of the $\delta_{as} SiD_3$ modes by coupling to ν_s-CSi_2 motion and must contribute most of the IR intensity to the band with a maximum at 733 cm^{-1}. However, $\nu_{24}(b_2)$, primarily a ρCH_2 mode, is also expected here. A likely A type band has a Q branch at 670.4 cm^{-1}, and this is confidently assigned to $\nu_{20}(b_1)$. A weak Q branch at 687.8 cm^{-1} may arise from $\nu_{19}(b_1)$ or $\nu_{25}(b_2)$. With only two reliable δSiH_3 or δSiD_3 assignments available, both associated with symmetric deformation, in the subsequent scaling of the force fields, it was necessary to assume identical scale factors for the δ_{as} and δ_s force constants.

(6) Silyl Rocking Motions. Figure 3 illustrates the imperfect nature of the d_0 contour associated with the $B_2(\nu_{25})$ band at 812 cm^{-1}. The QC calculations make it clear that the A_1 mode ν_7 cannot be at 595 cm^{-1} as previously assigned from the Raman spectrum but must instead underlie the distorted type A band at 763.4 cm^{-1} due to $\nu_{20}(b_1, \nu_{as}CSi_2)$. In d_6, there is slight evidence to suggest that the center of ν_{21} is a little lower than the Raman liquid values of 438 cm^{-1}. The band at 390 cm^{-1} previously assigned[1] to ν_{26} was not rerecorded.

(7) Fermi Resonance Correction. A small resonance is likely in the spectrum of d_6 between ν_4 at 1363 cm^{-1} and the combination $738(a_1) + 664(a_1)$, expected at 1402 cm^{-1}, but observed at 1407 cm^{-1}. Correcting ν_4 to 1368 cm^{-1} (Table 2) then increases the compatibility between the scaled d_0 and d_6 values of ν_4.

Force Field Scaling. The symmetry coordinates employed were identical to those employed for dimethylsilane, with exchange of silicon for carbon.[11] It was found possible to define 14 independent scale factors, as listed in Table 7 for each of the levels and basis sets employed. A high correlation coefficient of 0.92 was found between the factors for the strongly coupled ρCH_2 and ρSiH_3 motions in the B_2 symmetry species, and it was thought advisable to constrain these to be equal. There were slight indications in the case of the HF and MP2 force fields that this assumption was imperfect. However, with or without this constraint, the fit to the d_0 and d_6 B_2 frequencies remained poor, the cause of which was identified as incorrect values of the relatively large interaction force constant $F_{25,27}$ in all of the calculations. This was remedied by a manual adjustment of this constant prior to scaling, reducing it by between 8 and 15% according to the level of theory.

The 14 scale factors included independent ones for the two kinds of SiH bond stretching force constants, three such for silyl rocking constants, and two for the two silyl torsions. The A_2 and B_2 $\rho'' SiH_3$ factors would diverge further from each other if, as seems likely, the gas-phase value of ν_{13} (a_2) in d_6 lies below the liquid value of 417 cm^{-1}.

Table 7 includes for each set of factors for a particular calculation the average value, the standard deviation, and the range. However, the two torsional factors were excluded from these comparisons for two reasons. The first reason was the present uncertainty in the assignment of the torsional frequencies, and the second, the highly anomalous values which these factors exhibit in most cases. The size of the factor for the A_2 constant from the MP2/*tz*+ calculation, 3.11, is unprecedented in our experience. Anomalies such as these will remain even if a drastic revision in the frequencies becomes necessary. Thus, were an MP2 calculation to give more reasonable torsional factors as the result of reassignment, the B3LYP ones would then become unacceptable.

Without the torsions, the ranges and standard deviations for the various calculations are similar, with a slight preference for

TABLE 8: Potential Energy Distributions (PED) in DSM-d_0 and -d_6 from the Scaled B3LYP/*tz* Calculation

		DMS-d_0			DMS-d_6		
		ν_{calc}	P. E. D.[a]	main component	ν_{calc}	P. E. D.[a]	main component
A_1	ν_1	2903.7	$101S_4$	ν_sCH_2	2903.7	$101S_4$	ν_sCH_2
	ν_2	2167.7	$17S_1$, $82S_2$	$\nu SiH^a{}_2$	1565.5	$67S_1$, $35S_2$	$\nu_{as}SiD_3$
	ν_3	2166.2	$83S_1$, $18S_2$	ν_sSiH^s	1543.5	$34S_1$, $65S_2$	ν_sSiD_3
	ν_4	1368.7	$103S_9$	δ_sCH_2	1368.3	$103S_9$	δ_sCH_2
	ν_5	959.8	$11S_5$, $89S_6$	δ_sSiH_3	737.6	$35S_3$, $61S_6$	δ_sSiD_3
	ν_6	955.5	$91S_5$, $11S_6$	$\delta_{as}SiH_3$	689.3	$93S_5$	$\delta_{as}SiD_3$
	ν_7	778.6	$19S_3$, $66S_7$	$\rho'SiH_3$	662.1	$17S_3$, $9S_5$, $33S_6$, $34S_7$	coupled
	ν_8	548.9	$78S_3$, $23S_7$	ν_sCSi_2	467.8	$48S_3$, $46S_7$	coupled
	ν_9	175.4	$19S_7$, $108S_8$	δCSi_2	156.2	$25S_7$, $106S_8$	δCSi_2
A_2	ν_{10}	2161.9	$100S_{10}$	$\nu SiH^a{}_2$	1561.7	$101S_{10}$	$\nu SiD^a{}_2$
	ν_{11}	1048.3	$85S_{14}$	τCH_2	1031.2	$92S_{14}$	τCH_2
	ν_{12}	953.1	$101S_{11}$	$\delta_{as}SiH_3$	683.7	$102S_{11}$	$\delta_{as}SiD_3$
	ν_{13}	555.1	$106S_{12}$, $26S_{14}$	$\rho"SiH_3$	417.0	$110S_{12}$, $19S_{16}$	$\rho"SiD_3$
	ν_{14}	78.5	$104S_{13}$	τSiH_3	55.8	$104S_{13}$	τSiD_3
B_1	ν_{15}	2164.1	$90S_{15}$, $11S_{16}$	νSiH^s	1563.3	$72S_{15}$, $30S_{16}$	$\nu_{as}SiD_3$
	ν_{16}	2159.2	$10S_{15}$, $89S_{16}$	$\nu SiH^a{}_2$	1536.4	$29S_{15}$, $70S_{16}$	ν_sSiD_3
	ν_{17}	1057.8	$23S_{17}$, $80S_{21}$	wCH_2	1043.4	$24S_{17}$, $87S_{21}$	wCH_2
	ν_{18}	950.1	$100S_{18}$	$\delta_{as}SiH_3$	767.8	$78S_{17}$, $11S_{21}$	$\nu_{as}CSi_2$
	ν_{19}	916.8	$101S_{19}$	δ_sSiH_3	682.6	$99S_{18}$	$\delta_{as}SiD_3$
	ν_{20}	766.4	$79S_{17}$, $11S_{21}$	$\nu_{as}CSi_2$	666.7	$92S_{19}$	δ_sSiD_3
	ν_{21}	579.8	$97S_{20}$, $18S_{21}$	$\rho'SiH_3$	434.8	$102S_{20}$, $13S_{21}$	$\rho'SiD_3$
B_2	ν_{22}	2946.2	$101S_{23}$	$\nu_{as}CH_2$	2946.1	$101S_{23}$	$\nu_{as}CH_2$
	ν_{23}	2168.1	$100S_{22}$	$\nu SiH^a{}_2$	1566.8	$100S_{22}$	$\nu SiD^a{}_2$
	ν_{24}	958.0	$102S_{24}$	$\delta_{as}SiH_3$	736.4	$24S_{25}$, $50S_{27}$	ρCH_2
	ν_{25}	810.7	$42S_{25}$, $33S_{27}$	$\rho"SiH_3$	686.9	$101S_{24}$	$\delta_{as}SiD_3$
	ν_{26}	463.7	$65S_{25}$, $74S_{27}$	ρCH_2	390.0	$82S_{25}$, $55S_{27}$	$\rho"SiD_3$
	ν_{27}	133.0	$93S_{26}$	τSiH_3	104.0	$92S_{26}$	τSiD_3

[a] Diagonal terms ≥9%.

the B3LYP force fields. The sums of weighted squares of errors for the fit to the frequency data are also similar, reflecting the comparable fit data of Table 2. The apparent slight superiority of the fit with the HF calculations is offset by their failure outlined above in the prediction of νSiH values.

The need for a range of independent scale factors is present in all cases, even for motions as apparently similar as the two kinds of SiH stretching or the three involving silyl rocking. Substantial differences are also needed in the factors for the deformation, rocking, and wagging constants associated with the CH_2 group. In all of the treatments, the minimum value for any factor is associated with the CH_2 wag, wCH_2, which means that all are tending to calculate this frequency too high.

For a quantitative description of the vibrational modes in terms of the potential energy distributions (PED), results of the B3LYP/*tz* calculation are cited in Table 8. The scaled B3LYP/*tz* force field is given in Table 3S of the Supporting Information. The MP2/*tz*-based PED has slightly more coupling between wCH_2 and $\nu_{as}CSi_2$ motion in the B_1 modes ν_{17} and ν_{20} (d_0) and their counterparts ν_{17} and ν_{18} in d_6 and also between δ_sSiD_3 and $\delta_{as}SiD_3$ in d_6.

Prediction of Unknown or Uncertain Frequencies. Apart from the variations in prediction of νSiH and silyl torsional frequencies discussed above, the MP2/*tz* calculation is notable for a low value of ν_1 and a high value of ν_7 (d_o). The former is associated with a lower valence interaction force constant involving the stretchings of two CH bonds sharing the same carbon atom (see further below).The B3LYP or HF predictions are preferred because they yield more acceptable Fermi resonance shifts on ν_1.

Elsewhere, there is broad agreement between the predictions in Table 2 from the three levels of theory for the silyl deformations ν_5, ν_6, and ν_{12}. It is interesting to note the inversion of the symmetric and antisymmetric deformations δ_sSiH_3 and $\delta_{as}SiH_3$ that occurs in d_0 from the A_1 to the B_1 species, which is enhanced in d_6 due to the greater coupling there between the δ_sSiD_3 and ν_sSiC_2 motions.

Prediction of the position of the silyl rocking mode ν_7 in d_0 is more variable, the MP2 value of about 786 cm^{-1} lying 7 cm^{-1} higher than the B3LYP value of 778 cm^{-1}. The value of ~555 cm^{-1} predicted for the A_2 silyl rock ν_{13} is based on the liquid-phase Raman frequency seen in d_6 and may differ significantly from its actual position in the gas. Variations due to basis set are negligible in all of these predictions. The main source of error will lie in the constraints applied to the scale factors.

Unscaled Valence Stretching Interaction Force Constants. The full set of unscaled valence stretching force constants is given in Table 4S. Quoted here in Table 9 are the interaction constants f' which fall into three categories, α or gem constants, involving a central atom common to both bonds, β constants which relate bonds either gauche or trans (antiperiplanar) with respect to each other, and longer range γ constants between bonds separated by a motionless atom, in this case the SiH bonds in different silyl groups.

Among the α constants, there is a contrast between a reasonable agreement between MP2 and B3LYP values for SiH bonds, with the marked fall in value for the CH bond when an MP2 value is compared with an HF or B3LYP one. This is the basis for the larger $\nu_{as}CH_2/\nu_sCH_2$ splitting predicted from an MP2 calculation, which in turn yields an improbable Fermi resonance correction on ν_sCH_2. The same trend is found with the CH/CSi and CSi/CSi interactions, but not the SiH/SiH one.

This characteristic of MP2 calculations has been noted previously on a number of occasions.[11,17,18,23,26] It seemed profitable to explore how widespread the phenomenon might be. Table 10 shows a comparison of gem f' values from B3LYP and MP2 calculations for 17 molecules containing CH_3 and/or CH_2 groups. In almost every case the MP2 value is substantially below the B3LYP one. The apparent universality of this effect

TABLE 9: Unscaled Valence Stretching Interaction Force Constants f' (aJ Å^{-2}) in DSM

bond(s)[a]	f' type[b]	HF/*sv*	HF/*tz*	MP2/*sv*	MP2/*tz*	MP2/*tz*+	B3LYP/*sv*	B3LP/*tz*	B3LYP/*tz*+	B3LP/*cc*
SiH^a/SiH^a	α	0.0437	0.0461	0.0260	0.0322	0.0329	0.0252	0.0283	0.0287	0.0271
SiH^s/SiH^a	α	0.0444	0.0471	0.0267	0.0329	0.0334	0.0262	0.0293	0.0295	0.0281
SiH^s/SiH$^{s'}$	γ	0.0072	0.0060	0.0053	0.0047	0.0048	0.0051	0.0042	0.0043	0.0040
SiH^s/SiH$^{a'}$	γ	0.0023	0.0019	0.0014	0.0014	0.0014	0.0017	0.0016	0.0016	0.0014
SiH^{a1}/SiH$^{a1'}$	γ	0.0126	0.0105	0.0091	0.0080	0.0080	0.0098	0.0082	0.0083	0.0083
SiH^{a1}/SiH$^{a2'}$	γ	0.0010	0.0010	0.0004	0.0006	0.0005	0.0007	0.0008	0.0007	0.0007
SiH^s/SiC	α	0.0563	0.0605	0.0509	0.0544	0.0539	0.0442	0.0491	0.0495	0.0487
SiH^a/SiC	α	0.0549	0.0602	0.0481	0.0542	0.0546	0.0418	0.0475	0.0480	0.0475
SiH^s/SiC	β(t)	−0.0151	−0.0136	−0.0127	−0.0113	−0.0112	−0.0132	−0.0118	−0.0119	−0.0114
SiH^a/SiC	β(g)	−0.0164	−0.0145	−0.0153	−0.0142	−0.0141	−0.0134	−0.0120	−0.0121	−0.0120
SiH^s/CH	β(g)	0.0076	0.0070	0.0028	0.0028	0.0031	0.0053	0.0050	0.0051	0.0049
SiH^{a1}CH	β(g)	0.0078	0.0071	0.0031	0.0030	0.0031	0.0055	0.0051	0.0051	0.0050
SiH^{a2}/CH	β(t)	−0.0046	−0.0045	−0.0064	−0.0054	−0.0055	−0.0069	−0.0066	−0.0066	−0.0066
CH/CH	α	0.0396	0.0395	0.0090	0.0090	0.0088	0.0283	0.0332	0.0335	0.0342
CH/CSi	α	0.0289	0.0282	0.0149	0.0109	0.0100	0.0276	0.0330	0.0327	0.0351
CSi/CSi	α	0.0679	0.0764	0.0572	0.0669	0.0648	0.0669	0.0794	0.0789	0.0802

[a] a′, a1′, and a2′ denote hydrogen atoms in SiH bonds in the second silyl group; a1 and a1′ lie on the same side of the skeletal plane, and a1 and a2′ lie on opposite sides. [b] $f_{\beta g}'$ involves SiH and SiC or CH bonds oriented gauche toward each other; $f_{\beta t}'$ involves similar bonds trans (antiperiplanar) related.

TABLE 10: Comparison of Unscaled CH Stretch/CH Stretch Interaction Constants f'(aJ Å^{-2}) from B3LYP and MP2 Treatments[a]

molecule	basis	group[b]	B3LYP	MP2
CH_4	*tz*		0.036	0.013
CH_3F	*tz*	CH_3	0.054	0.033
CH_3Cl	*tz*	CH_3	0.037	0.022
C_2H_6	*tz*	CH_3	0.051	0.024
CH_3CH_2F	*tz*	CH_3	0.040, 0.044	0.013, 0.018
		CH_2	0.065	0.042
$CH_3CH_2CH_3$	*tz*+	CH_3	0.048, 0.049	0.021, 0.022
		CH_2	0.064	0.033
$CH_3CH_2SiH_3$	*tz*	CH_3	0.052, 0.048	0.026, 0.022
		CH_2	0.048	0.021
CH_3SiH_3	*tz*	CH_3	0.035	0.011
$(CH_3)_2SiH_2$	*sv*	CH_3	0.033, 0.033	0.012, 0.013
$(CH_3)_3SiH$	*sv*	CH_3	0.033, 0.033	0.012, 0.012
CH_2F_2	*tz*	CH_2	0.059	0.042
CH_2Cl_2	*tz*	CH_2	0.039	0.034
$CH_2(SiH_3)_2$	*tz*	CH_2	0.033	0.009
FCH_2SiH_3	*tz*	CH_2	0.052	0.031
$ClCH_2SiH_3$	*tz*	CH_2	0.039	0.023
$CH_2{=}CH_2$	*tz*+	CH_2	0.034[c]	0.013
$CH_2{=}CF_2$	*tz*+	CH_2	0.014	−0.007

[a] This work. [b] In asymmetric methyl groups, the two f' values are listed in the order CH_a/CH_s and CH_a/CH_a. [c] CCSD(T)/cc-pVTZ calculations yield a slightly lower value (0.028 aJ Å^{-2}),[35] whereas local mode studies place it higher (∼0.044 aJ Å^{-2}).[36]

suggests that MP2 calculations should be avoided if a close analysis of CH_3 or CH_2 stretching vibrations is to be attempted, a fact not commonly appreciated.

The β interactions fall into two categories. Those between the CH and SiH bonds exhibit the familiar pattern of positive gauche interactions and smaller, negative trans ones.[18] The two gauche interactions are both smaller from an MP2 calculation.

However, the β interactions between SiC and SiH bonds are negative and very similar in size for both gauche- and trans-related pairs, with little variation with level and basis set.

The largest of the γ interactions, $f_{a1a1'}$, operates between SiH bonds roughly parallel to each other in the two silyl groups and is larger than either of the β constants. The other γ constants are either comparable in size to the β ones or much smaller. However, all are calculated consistently positive throughout. Further light on the way these γ constants vary with level of theory and basis set and also with bond orientation is thrown by the calculations of dipole/dipole interactions described below.

Centrifugal Distortion Constants. Results for these from MP2 and B3LYP calculations are listed in Table 11. They show a significant dependence on both basis and level of theory, but may be found of use in guiding future microwave investigations. No experimental values are currently available.

Electrical Properties of the SiH Bonds. Table 12 lists the atomic polar tensors for DSM from the B3LYP/*tz* calculation. For the silicon and hydrogen atoms, the reference axes have been rotated so that the *z* axis lies along the direction of the bond containing the atom. In such a case, in the zero order optical parameter approximation, $\partial p_x/\partial x$ ($= p_{xx}$) and $\partial p_y/\partial y$ ($= p_{yy}$), which relate to bending of the bond concerned, would both equal μ/r, where μ is the bond dipole moment and r the bond length, whereas $\partial p_z/\partial z$ ($= p_{zz}$) would be the dipole derivative with respect to stretching of the bond, $\partial\mu/\partial r$.[37] Nonzero values of $\partial p_x/\partial z$ and $\partial p_y/\partial z$ indicate the extent to which the vector $\partial\mu/\partial r$ in fact is directed away from the bond direction. As usual

TABLE 11: Centrifugal Distortion Constants (kHz) for DSM-d_0 and -d_6

constant	MP2/*sv*	MP2/*tz*	MP2/*tz*+	B3LYP/*sv*	B3LYP/*tz*	B3LYP/*tz*+
			d_0			
D_J	1.6917	1.6410	1.6337	1.6045	1.5574	1.5579
D_{JK}	−15.6369	−16.1861	−16.0732	−15.6359	−15.9476	−15.9120
D_K	122.6594	131.5618	131.0556	125.6571	133.2564	133.0394
d_1	−0.2255	−0.2145	−0.2130	−0.2112	−0.2019	−0.2020
d_2	0.0021	0.0020	0.0020	0.0019	0.0019	0.0019
			d_6			
D_J	1.1594	1.1292	1.1246	1.1014	1.0697	1.0701
D_{JK}	−1.7633	−2.0919	−2.0942	−2.0128	−2.1042	−2.0730
D_K	27.4449	29.3685	29.2427	28.2704	29.6788	29.59
d_1	−0.1248	−0.1194	−0.1185	−0.1175	−0.1126	−0.1126
d_2	0.0063	0.0057	0.0057	0.0057	0.0054	0.0054

TABLE 12: Atomic Polar Tensors (e) in DSM, from B3LYP/*tz* Calculations

	C(1)[a,b]			Si(2)[c,d]			H(4)[b,c]		
	∂x	∂y	∂z	∂x	∂y	∂z	∂x	∂y	∂z
∂p_x	−0.880	0.000	0.000	0.909	0.000	0.186	0.041	0.000	0.000
∂p_y	0.000	−0.412	0.000	0.000	0.953	0.000	0.000	0.058	−0.013
∂p_z	0.000	0.000	−0.484	−0.035	0.000	1.429	0.000	−0.041	−0.088
	H^s(6)[c,d]			H^a(7)[c,e]					
∂p_x	−0.295	0.000	0.052	−0.216	0.011	0.004			
∂p_y	0.000	−0.212	0.000	0.020	−0.280	−0.046			
∂p_z	0.077	0.000	−0.349	−0.003	−0.002	−0.296			

[a] *z* axis along C_2 symmetry axis. [b] *x* axis in the CSi_2 plane. [c] *z* axis along the C−Si(2), C−H(4), Si−H(6), or Si−H(7) bond. [d] *y* axis in the CH_2 plane. [e] *x* and *y* axes in arbitrary orientation.

TABLE 13: Infrared Stretching Intensities and Electrical Properties Associated with Some SiH Bonds, from B3LYP/*tz* Calculations[a]

	SiH_4[b]	$MeSiH_3$[b]	Me_2SiH_2[b]	Me_3SiH[b]	Si_2H_6	DSM (H^s)	DSM (H^a)	DSM average	SiH_2Cl_2
A_{av}[c] obs	70(1)[d]	102(5)[e]	127(6)[e]		72(4)[e]			90(3)[e]	67(2)[e]
A_{av}[c] calc	91.0	120.0	144.9	167.3	89.8			114.8	74.8
A^{is} [f]	94.9	122.7	146.3	167.3	93.0	136.9	103.7		75.7
$\partial\mu/\partial r$[g]	−0.287	−0.329	−0.361	−0.387	−0.293	−0.353	−0.300		−0.242
θ[h]	0.0	4.8	4.1	0.0	9.1	8.4	0.8, 8.8		7.2
q_H[i]	−0.126	−0.139	−0.150	−0.154	−0.114	−0.133	−0.132		−0.088
χ_H[j]	0.248	0.280	0.308	0.330	0.262	0.296	0.268		0.272
$\bar{p}_H$[k]	−0.246	−0.277	−0.304	−0.327	−0.253	−0.285	−0.264		−0.269
$\bar{p}_\perp$[l]	−0.226	−0.251	−0.276	−0.298	−0.235	−0.254	−0.248		−0.284

[a] This work, except where otherwise indicated. [b] Reference 11, with transcription errors corrected. [c] Average infrared intensity (km mol^{-1}) observed (obs) or calculated (calc) in the νSiH region of the parent molecule, divided by the number of SiH bonds. [d] Reference 38. [e] Reference 12. [f] QC-calculated infrared intensity (km mol^{-1}) for the ν^{is}SiH band. [g] Dipole derivative (e) for stretching of the Si−H bond. [h] Angle(s) (degrees) made between $\partial\mu/\partial r$ and the Si−H bond direction. [i] Mulliken charge on H. [j] King atomic charge, $= \mathrm{Tr}\{\mathbf{P'}_A \cdot \mathbf{P}_A\}/3$.[39] [k] Mean atomic charge, $= (p_{xx} + p_{yy} + p_{zz})/3$.[39] [l] Mean bending charge, $= (p_{xx} + p_{yy})/2$, when the *z* axis lies along the Si−H bond.[18]

TABLE 14: Dipole−Dipole Potential Energies DPE (10^3 e^2 $Å^{-1}$) Involved in the Simultaneous Stretchings of SiH Bonds in Neighboring Silyl Groups, from QC Calculations

	SiH^s/ $SiH^{s'}$	SiH^s/ $SiH^{a'}$	SiH^{a1}/$SiH^{a1'}$	SiH^{a1}/$SiH^{a2'}$
HF/*sv*	1.982	−0.423	4.362	−0.728
HF/*tz*	1.521	−0.318	3.218	−0.544
MP2/*sv*	1.491	−0.326	3.265	−0.538
MP2/*tz*	1.233	−0.272	2.660	−0.445
MP2/*tz*+	1.248	−0.273	2.669	−0.446
B3LYP/*sv*	1.463	−0.301	3.067	−0.507
B3LYP/*tz*	1.172	−0.240	2.376	−0.397
B3LYP/*tz*+	1.197	−0.245	2.413	−0.406
B3LYP/*cc*	1.149	−0.234	2.294	−0.382

for CH bonds, p_{xx} and p_{yy} are both positive, but p_{zz} is negative. However, the hydrogen in an SiH bond carries a negative charge in both stretching and bending motions.

Electrical properties derived from these atomic polar tensors for the SiH bonds in DSM are compared in Table 13 with those in silane, disilane, three methylsilanes, and dichlorosilane. Also included are the average SiH stretching infrared intensities, per bond, derived experimentally and from B3LYP/*tz* calculations for each parent molecule. The latter differ trivially from the computed intensities of the ν^{is}SiH band, also cited. Although, as has already been noted, the computed ν^{is}SiH band intensities for the SiH^s and SiH^a bonds in DSM differ markedly from each other, the computed average intensity per bond occupies a position between those for the SiH bonds in silane and methylsilane, as does the experimental average value. The rise in νSiH intensity is readily attributable to the increased negative charge on the hydrogen atom expected from the inductive effect of the methyl or CH_2 group. However, it is interesting to note that in DSM the H^s atom is much more affected in this way than the H^a atom. The Mulliken charge q_H, also quoted in Table 13, follows the same trend from silane to methylsilane, but the difference between H^s and H^a in DSM seems less marked. An opposite type of inductive effect due to chlorine shows up in the computed and observed intensities for the SiH bond in SiH_2Cl_2. By contrast, the α effect of a second silyl group, as exhibited by the disilane data, is negligible.

As expected, values of $\partial\mu/\partial r$ parallel very closely changes in A_{av}. The direction of $\partial\mu/\partial r$ lies within 9° of that of the bond. Calculation of the mean bending charge[18] $\bar{p}_\perp = (p_{xx} + p_{yy})/2$ also shows the H^s atom to carry a more negative charge in its bending motion than the H^a atom, both falling in line with variations from silane to disilane and methylsilanes. However, the same is not true in the case of SiH_2Cl_2, where $\bar{p}_\perp$ rises markedly from silane, in contrast to the fall for $\partial\mu/\partial r$.

Long-Range Effects Between Bonds in DSM. *SiH/SiH Stretching*. The QC data obtained in this work permit an exploration of a possible relation between dipole/dipole forces and the SiH sretch−stretch interactions, which were suggested earlier as being responsible for splittings of the SiH stretching modes in the parent DSM molecule.[2]

As described in calculations for disilylamines,[8−10] the model employed assumes (1) that the dipole is proportional to the parameter $\partial\mu/\partial r$ for the bond concerned, (2) that the dipole is located at the position of the moving hydrogen atom, and (3) that the direction of the dipole is along the SiH bond. That the latter is approximately true is seen from the angle data in Table 13.

The potential energy DPE is given by the standard formula:[40]

$$\mathrm{DPE} = \mu_i \mu_j r^{-3}(\cos\theta_i \cos\theta_j - \sin\theta_i \sin\theta_j \cos\phi_{ij})$$

Here μ_i and μ_j are the two dipole moments concerned, equated to the values of $\partial\mu/\partial r$ for the two SiH bonds *i* and *j*, assuming the same unit amplitude in the stretching coordinate as for *f* ′, *r* is the distance between the two dipoles and θ_i, θ_j, and ϕ_{ij} are the angles $H_iSi_kSi_l$, $H_jSi_lSi_k$, and $H_iSi_kSi_lH_j$ (dihedral), respectively.

Table 14 lists the values of DPE obtained from the three levels of theory, for the four types of γ interaction possible. As might

TABLE 15: Hydrogen Interatomic Distances *R* (Å) and Mulliken Charges *q* (e) at Various Levels of Theory

	R (H_4-H_6)	R (H_4-H_7)	R (H_7-H_{10})	R (H_7-H_{11})	q_4	q_6	q_7
HF/*sv*	3.005	3.661	3.358	4.125	0.200	−0.146	−0.144
HF/*tz*	2.994	3.658	3.380	4.146	0.150	−0.196	−0.193
MP2/*sv*	3.025	3.672	3.277	4.067	0.200	−0.104	−0.102
MP2/*tz*	3.005	3.656	3.298	4.079	0.163	−0.166	−0.164
MP2/*tz*+	3.007	3.657	3.300	4.081	0.214	−0.151	−0.151
B3LYP/*sv*	3.028	3.682	3.334	4.116	0.186	−0.069	−0.069
B3LYP/*tz*	3.013	3.674	3.360	4.136	0.162	−0.133	−0.132
B3LYP/*tz*+	3.013	3.674	3.359	4.135	0.207	−0.121	−0.119
B3LYP/*cc*	3.014	3.670	3.342	4.120	0.103	−0.038	−0.037

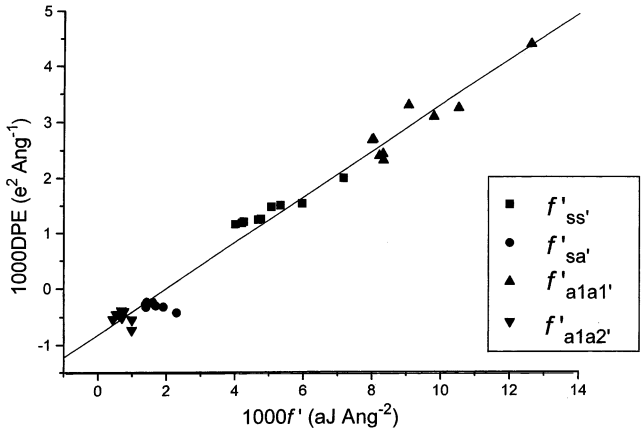

Figure 5. Correlation graph of the νSiH/νSiH interaction force constant f' (aJ Å^{-2}) operating between SiH bonds in different silyl groups, versus the dipole/dipole interaction energy DPE (e^2 Å^{-1}), both quantities from HF, MP2, and B3LYP calculations with the *sv*, *tz*, *tz*+, and *cc* basis sets. The line is described by the equation: $10^3\mathrm{DPE} = -0.810(54) + 0.408(10)\ 10^3 f'$; $R = 0.990$, $\sigma_d = 0.208$

be expected, the largest energy is associated with the SiH^{a1} and $SiH^{a1'}$ bonds which lie roughly parallel to each other. The general relation of these DPE values to the QC-based f' constants is demonstrated in Figure 5, which shows a good correlation between the two quantities, independent of wave function basis or level of theory. The gradient of 0.408 is close to the value of 0.433 expected for a purely electrostatic origin for f'.[10] This must be considered satisfactory in view of the three assumptions listed above. However, the influence of an additional factor is evident from the presence of a negative intercept on the DPE axis, which would be zero if only dipole−dipole forces were present. Nevertheless, the suggestion is strong that the HF, MP2 and B3LYP approaches agree in finding the main source of the stretch/stretch interactions to lie in dipole/dipole interactions.

Torsional Motion. The spread of points for a particular f' in Figure 5 is almost wholly due to the differing dipole derivatives yielded by the various calculations. It is then pertinent to enquire if differences in the calculated charge distributions on hydrogen can explain the variations in the A_2 torsional frequency seen in Table 6, particularly the low values from MP2 calculations.

Table 15 shows some of the factors which might be thought relevant. In addition to the Mulliken charges on the hydrogens in the CH bond (H_4) and SiH bonds (H^s_6, H^a_7), the distances H_4-H_6, H_4-H_7, H_7-H_{10}, and H_7-H_{11} are given. (The remote hydrogens H_6 and H_9 are much further apart and considered unlikely to influence torsional motion.) Changes in the distances listed are less than 1% for H_4-H_6 and H_4-H_7 and less than 3% for H_7-H_{10} and H_7-H_{10}. Although there is a dip in the latter from an HF value to an MP2 one, with a consequent rise from MP2 to B3LYP, the changes are so small as to make it rather unlikely that they can produce the torsional variation seen. The Mulliken charge on H_4 changes slightly with basis set but rather less with level of theory. There is a significant fall in the negative charge on each type of hydrogen attached to silicon, H_6 and H_7, in the sequence HF > MP2 >B3LYP, but this is not the order of the variation in the torsional constant. A further point is that the A_2 motion involves an in-phase rotation of both silyl groups in which changes in the repulsion between H^a atoms might be expected to be small. Repulsions between these atoms should be more noticeable in the B_2 torsional motion, but agreement on the frequency of the latter is in fact excellent between all levels of theory.

These considerations suggest that the reason for the anomalously low MP2 torsional force constant has yet to be discovered.

Acknowledgment. Professor D. W. H. Rankin and Dr S. L. Hinchley are warmly thanked for making available the Edinburgh ab initio facility for running the Gaussian 98 program. I thank also Professor H. Bürger for the data of Reference (32) and two referees for helpful comment.

Supporting Information Available: Infrared frequencies observed in $(SiH_3)_2CH_2$ (Table 1S) and $(SiD_3)_2CH_2$ (Table 2S); the B3LYP/6-311G** force field (Table 3S); unscaled valence stretching force constants for all of the QC calculations (Table 4S). This material is available free of charge via the Internet at http://pubs.acs.org.

References and Notes

(1) McKean, D. C.; Davidson, G.; Woodward, L. A. *Spectrochim. Acta* **1970**, *26A*, 1815.
(2) McKean, D. C.; Morrisson, A. R.; Torto, I.; Kelly, M. I. *Spectrochim. Acta* **1985**, *41A*, 25.
(3) Almenningen, A.; Seip, H. M.; Seip, R. *Acta Chem. Scand*. **1970**, *24*, 1697.
(4) Shiki, Y.; Kuginuki, Y.; Hasegawa, A.; Hayashi, M. *J. Mol. Spectrosc*. **1978**, *73*, 9.
(5) Schmidbaur, H.; Zech, J.; Rankin, D. W. H.; Robertson, H. E. *Chem. Ber*. **1991**, *124*, 1953.
(6) Hager, R.; Steigelmann, O.; Müller, G.; Schmidbaur, H.; Robertson, H. E.; Rankin, D. W. H. *Angew. Chem., Int. Ed. Engl.* **1990**, *29*, 201.
(7) McKean, D. C. unpublished work.
(8) Fleischer, H.; McKean, D. C.; Pulham, C. R.; Bühl, M. *J. Chem. Soc., Dalton Trans.* **1998**, 585.
(9) Fleischer, H.; McKean, D. C.; Parsons, S.; Bühl, M. *Z. Anorg. Allg. Chem*. **1999**, *625*, 313.
(10) Fleischer, H.; McKean, D. C.; Torto, I. *Spectrochim. Acta* **2002**, *58A*, 911.
(11) McKean, D. C.; Torto, I. *J. Mol. Spectrosc*. **2002**, *216*, 363.
(12) McKean, D. C.; Coats, A. M. unpublished work.
(13) Frisch, M. J.; Trucks, G. W.; Schlegel, H. B.; Scuseria, G. E.; Robb, M. A.; Cheeseman, J. R.; Zakrzewski, V. G.; Montgomery, J. A., Jr.; Stratmann, R. E.; Burant, J. C.; Dapprich, S.; Millam, J. M.; Daniels, A. D.; Kudin, K. N.; Strain, M. C.; Farkas, O.; Tomasi, J.; Barone, V.; Cossi, M.; Cammi, R.; Mennucci, B.; Pomelli, C.; Adamo, C.; Clifford, S.; Ochterski, J.; Petersson, G. A.; Ayala, P. Y.; Cui, Q.; Morokuma, K.; Malick, D. K.; Rabuck, A. D.; Raghavachari, K.; Foresman, J. B.; Cioslowski, J.; Ortiz, J. V.; Stefanov, B. B.; Liu, G.; Liashenko, A.; Piskorz, P.; Komaromi, I.; Gomperts, R.; Martin, R. L.; Fox, D. J.; Keith, T.; Al-Laham, M. A.; Peng, C. Y.; Nanayakkara, A.; Gonzalez, C.; Challacombe, M.; Gill, P. M. W.; Johnson, B. G.; Chen, W.; Wong, M. W.; Andres, J. L.; Head-Gordon, M.; Replogle, E. S.; Pople, J. A. *Gaussian 98*, revision A.7; Gaussian, Inc.: Pittsburgh, PA, 1998.

(14) (a) Dunning, T. H., Jr. *J. Chem. Phys*. **1989**, *90*, 1007. (b) Woon, D. E.; Dunning, T. H., Jr. *J. Chem. Phys*. **1993**, *98*, 1358.
(15) (a) Hedberg, L.; Mills, I. M. *J. Mol. Spectrosc*. **1993**, *160*, 117. (b) Hedberg, L.; Mills, I. M. *J. Mol. Spectrosc*. **2000**, *203*, 82.
(16) Pulay, P.; Fogarasi, G.; Pang, F.; Boggs, J. E. *J. Am. Chem. Soc*. **1979**, *101*, 2550.
(17) McGrady, G. S.; Downs, A. J.; Bednall, N. C.; McKean, D. C.; Thiel, W.; Jonas, V.; Frenking, G.; Scherer, W. *J. Phys. Chem. A* **1997**, *101*, 1951.
(18) McKean, D. C. *J. Mol. Struct*. **2002**, *642*, 25.
(19) McKean, D. C.; Torto, I. *Spectrochim. Acta* **2001**, *57A*, 1725.
(20) For example, see: (a) Rauhut, G.; Pulay, P. *J. Phys. Chem*. **1995**, *99*, 3093. (b) Baker, J.; Jarzecki, A. A.; Pulay, P. *J. Phys. Chem. A* **1998**, *102*, 1412. (c) Baker, J.; Pulay, P. *J. Comput. Chem*. **1998**, *19*, 1187.
(21) McKean, D. C. *J. Phys. Chem A* **2000**, *104*, 8995.
(22) McKean, D. C.; Palmer, M. H.; Guest, M. F. *J. Mol. Struct*. **1996**, *376*, 289.
(23) Fleischer, H.; McKean, D. C.; Torto, I.; Boggs, J. E. *J. Mol. Struct*. **2002**, *604*, 221.
(24) Mathews, S.; Duncan, J. L.; McKean, D. C.; Smart, B. A. *J. Mol. Struct*. **1997**, *413*−*414*, 553.
(25) Murphy, W. F.; Zerbetto, F.; Duncan, J. L.; McKean, D. C. *J. Phys. Chem*. **1993**, *97*, 581.
(26) McKean. D. C. *Spectrochim. Acta* **1999**, *55A*, 1485.
(27) McKean, D. C. *Spectrochim. Acta*, **1992**, *48A*, 1335. A νMD fundamental frequency results from a transition to a lower level in the anharmonic potential well than that for the MH bond and so is less affected by the anharmonicity. If the νMH stretching force constant in a quadratic force field is refined to the observed νMH value, the νMD frequency will be calculated too low. A quantitative basis for this effect is expressed in Dennison's Rule for the interrelation of the frequencies of stretching modes of bonds involving isotopomers.[28]
(28) (a) Dennison, D. M. *Rev. Mod. Phys*. **1940**, *12*, 175. (b) Hansen, G. E.; Dennison, D. M. *J. Chem. Phys*. **1952**, *20*, 313.
(29) Church, J. S.; Durig, J. R.; Mohamed, T. A.; Mohamed, A. B. *Spectrochim. Acta* **1994**, *50A*, 639.
(30) Durig. J. R.; Church, J. S. *J. Chem. Phys*. **1980**, *73*, 4784.
(31) Jagannath, H.; Ozier, I.; Moazzen-Ahmadi, N. *J. Mol. Spectrosc*. **1986**, *119*, 313.
(32) Moritz, P. Thesis, Universität-Gesamthochschule Wuppertal, 1992.
(33) Durig, J. R.; Hawley, C. W. *J. Chem. Phys*. **1973**, *59*, 1.
(34) Mohamed, T. A.; Guirgis, G. A.; Nashed, Y. E.; Durig, J. R. *Struct. Chem.* **1998**, *9*, 255.
(35) Martin, J. M. L.; Lee, T. J.; Taylor, P. R.; François, J.-P. *J. Chem. Phys.* **1995**, *103*, 2589.
(36) Duncan, J. L. *Spectrochim. Acta* **1991**, *47A*, 1.
(37) Newton, J. H.; Person, W. B. *J. Chem. Phys*. **1976**, *64*, 3036.
(38) Coats, A. M.; McKean, D. C.; Steele, D. *J. Mol. Struct*. **1994**, *320*, 269.
(39) King, W. T.; Mast, G. B. *J. Phys. Chem*. **1976**, *80*, 2521.
(40) Buckingham, A. D. *Quart. Rev.* **1959**, *13*, 183.